



## **Geo-electric Laboratory Simulation for Characterization of Hydrocarbon Impacted Coastal Sands**

**S. Sualla<sup>1</sup>, M. N. Tijani<sup>2</sup>, M. A. Oladunjoye<sup>2</sup> and O. A. Oki<sup>3\*</sup>**

<sup>1</sup>Total Quality Integrated Services Ltd, Rivers State, Nigeria.

<sup>2</sup>Department of Geology, University of Ibadan, Oyo State, Nigeria.

<sup>3</sup>Department of Geology, Niger Delta University, Bayelsa State, Nigeria.

### **Authors' contributions**

*This work was carried out in collaboration between all authors. Authors SS and MNT designed the study, performed the statistical analysis, wrote the protocol and wrote the first draft of the manuscript.*

*Authors MAO and OAO managed the analyses of the study. Authors SS and OAO managed the literature searches. All authors read and approved the final manuscript.*

### **Article Information**

DOI: 10.9734/ACRI/2018/37490

#### Editor(s):

- (1) Wang Mingyu, School of Metallurgy and Environment, Central South University, China.  
(2) Sivakumar Manickam, Professor, Chemical and Nanopharmaceutical Process Engineering, Associate Dean, Research and Knowledge Exchange, Nanotechnology and Advanced Materials (NATAM), The University of Nottingham Malaysia Campus, Malaysia.

#### Reviewers:

- (1) Agbasi Okechukwu Ebuka, Michael Okpara University of Agriculture, Nigeria.  
(2) Aigbedion Isaac, Ambrose Alli University, Nigeria.  
(3) Ojewumi Modupe Elizabeth, Covenant University, Nigeria.

Complete Peer review History: <http://www.sciencedomain.org/review-history/22835>

**Original Research Article**

**Received 19<sup>th</sup> September 2017**

**Accepted 3<sup>rd</sup> December 2017**

**Published 24<sup>th</sup> January 2018**

### **ABSTRACT**

An electrical resistivity experiment was undertaken using a laboratory model tank with the aim of simulating and characterizing hydrocarbon spills on coastal sands. Prior to injection of fluids, geo-electric measurements were done as a control, subsequently injection of crude oil into the model tank was undertaken and geo-electric measurements carried out. Seven (7) electrical traverse lines were established in the tank and measurements were taken for two (2) scenarios of baseline environment and hydrocarbon impacted environment making a total of fourteen (14) geo-electric profiles. Measurements were made using dipole-dipole array, and inversion using DIPRO software to obtain the 2-D geo-electrical models. Textual and hydraulic characterization showed the medium was well sorted fine to medium grain sand. Pre-injection inverted data obtained for all the traverses

\*Corresponding author: Email: [ustin\\_oki@yahoo.com](mailto:ustin_oki@yahoo.com), [ustin\\_oki@mail.ndu.edu.ng](mailto:ustin_oki@mail.ndu.edu.ng);

revealed that the porous medium exhibited heterogeneity which was more evident on traverse 5, 6 and 7 compared to traverse 1, 2, 3, and 4. Images obtained showed high resistive anomaly reflected the presence of crude oil plume within the coastal sand. Resistivity profiles along the main lines showed migration of the hydrocarbon plume was more prominent along traverse 6 and 7, due to high hydraulic conductivity sands. Also, in comparison to the orthogonal lines, traverses 1, 2, 3 and 4 clearly delineated hydrocarbon plumes. Results from this study demonstrated a successful application geo-electric investigation for characterization of hydrocarbon spills in the soil, which would aid efficient remediation designs.

*Keywords: Laboratory simulation; electrical resistivity; coastal sand; hydrocarbon contamination.*

## 1. INTRODUCTION

One of the biggest problems of environmental concern in the coastal oil producing communities in Nigeria is oil spillage. 4,800 oil spills were recorded between 1960 and 2010 [1]. Oil spills not only degrades fertile farmlands, it also contaminates surface and underground water bodies, destroying the ecosystem and rendering the local economy unproductive over very long periods of time. In order for remediation of contaminated soil and groundwater systems to be effective, it is important to precisely detect and delineate spill impacted areas within the subsurface environment. Drilling and chemical analysis for detection of the contaminated subsoil and groundwater system may be essential, but are usually expensive and time consuming. Geophysical methods offer a relatively fast, non-invasive, cost effective and efficient process for characterizing hydrocarbon contaminant plumes in the subsurface. Ground Penetrating Radar, Electromagnetic and Electrical Resistivity investigations have been employed by several researchers to characterize hydrocarbon spill sites with great success [2,3,4,5,6,7,8,9].

The use of electrical methods is based on the premise that the presence of contaminants in the subsurface will have a distinct resistivity contrast with the surrounding uncontaminated host environment [10]. This contrast may be based on several factors such as particle size distribution, void ratio, soil moisture, lithology and fabric which typically make up the different constituents of the affected zone [11,12]. However for organic contaminants that is not miscible with water such as crude oil and the complexity of physico-chemical reactions with the host environment makes it unrealistic to determine a typical range of resistivity which could enable differentiation of the plume from its surroundings. These phenomena can significantly affect the electrical

properties of soil and groundwater and make clear and unambiguous detection of the contaminants quite difficult [13]. Although hydrocarbons usually show very high resistivity values, the electrical behaviour of the hydrocarbons in soil or groundwater can be affected by biodegradation and can lead to remarkable variations in the dissolved ions in the fluid phase of the subsoil. This phenomenon usually leads to an increase in the conductivity of the zone affected by the plume [14].

This research simulates hydrocarbon spills on coastal sands in a laboratory model-box, a characterization of spills using electrical method was then investigated as a measure of spill cleanup design.

## 2. METHODOLOGY

The electrical resistivity method involves the determination of the subsurface resistivity distribution, by taking measurements on the ground surface. This process entails the passage of electrical current (I), into the ground by means of current electrodes (usually two), and measuring the potential difference ( $\Delta V$ ) between two potential electrodes. Thus, by measuring  $\Delta V$  and I, and knowing the geometric factor (G), which takes into account the geometric spread of the electrode array configuration, the resistivity value ( $\rho$ ) of the subsurface formation can be obtained. It is important to note that what is actually measured either in the laboratory or field is the apparent resistivity ( $\rho_a$ ), and is shown in the equation below:

$$\rho_a = \frac{\Delta V}{I} \cdot G \quad (1)$$

Electrical characteristic is also commonly described by the conductivity  $\sigma$  ( $\text{Sm}^{-1}$ ) which is equivalent to the reciprocal of the soil resistivity. Thus:

$$\sigma = \frac{1}{\rho} \quad (2)$$

The measured apparent resistivity data can be converted to a true geologic model of the subsurface through inversion. The geologic subsurface condition, characteristics of materials in the subsurface, and the presence and movement of contaminant can be inferred from the resistivity measurement [15].

In the present study, the dipole-dipole electrode array was used (Fig. 1). The array is made up of four collinear electrodes; two current electrodes (C1 and C2 or A and B), and two potential electrodes (P1 and P2 or M and N). In this electrode array, the potential electrodes are closely spaced and remote from the current electrodes, which also are closely spaced together (Fig. 1). This arrangement of electrodes has the advantage of low inductive coupling between the potential and current cables during survey. The spacing between the current electrode pair C1-C2 is given as  $a$  and is the same distance as between the potential electrodes P1-P2. There is another factor that is taken into consideration in this array known as  $n$ .

This factor represents the ratio of the distance between the C1 and P1 electrodes to the C2-C1 or P1-P2 dipole length  $a$ . Usually, with this array, the electrode spacing  $a$  is kept fixed while the  $n$  factor is increased from 1 to 2, in some cases up to six, in order to increase the depth of investigation. The dipole-dipole is very sensitive to horizontal changes but not so sensitive to vertical changes in resistivity. It is thus better at

mapping vertical structures than horizontal structures. One of the possible disadvantages of dipole-dipole array system is the small signal strength for large values of the  $n$  factor [16]. The electrode separation  $a$  was taken as 2 cm (orthogonal traverses) and 4 cm (main traverses) while  $n$  varied from 1 to 5.

The geometric factor ( $G$ ) is given as;

$$G = \pi a(n + 1)(n + 2)n \quad (3)$$

Thus, the apparent resistivity equation for the dipole-dipole array is given by;

$$\rho_a = \pi R a \{(n + 1)(n + 2)\} \quad (4)$$

where  $a$  is the dipole length,  $R$  is the measured soil (coastal sand) resistance, and  $n$  is a constant that varies from 1 to 5.

## 2.1 Experimental Setup

Laboratory model studies in this research involved the simulation of a freshwater subsurface environment which was impacted by crude oil. The model tank used for the experiment was made of plank, strong enough to withstand the pressure of the sand fill. The tank is 150 cm long, 70 cm wide and 90 cm deep (Fig. 1). Its interior was lined with polythene, to prevent seepage of saturating fluid into the wooden tank during the course of the experiment. The tank was filled to 50 cm with coastal sand that has been previously mixed with clay to effectively model the field situation.

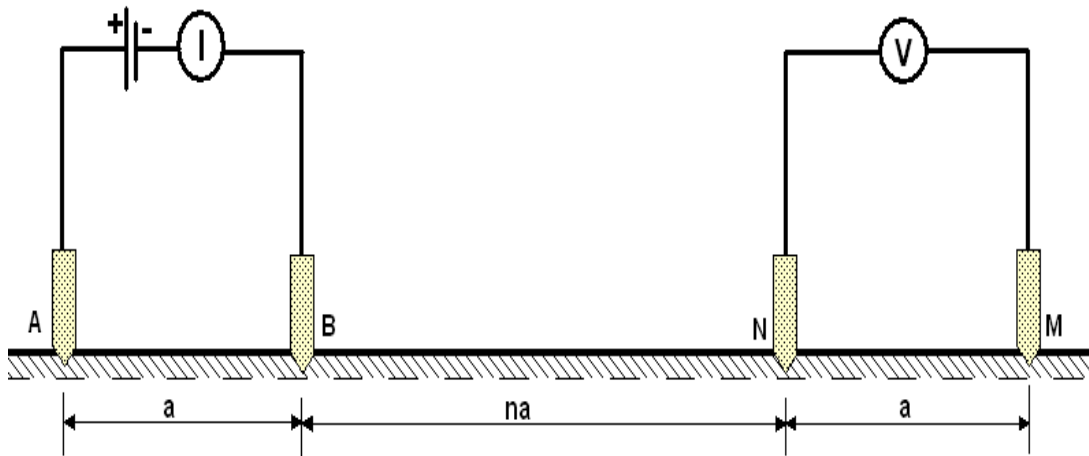


Fig. 1. Dipole-dipole electrode configuration

Prior to filling the coastal sand into the model tank its textural (grain-size distribution analysis) and hydraulic (transmissivity) characteristics was determined by weighing 500 g of a sun-dried sample of the sand with a digital balance which was poured into a set of sieves (largest diameter on top and smallest at the bottom). The various constituents material retained on each sieve after been subjected to a mechanical shaker machine for 10 minutes were weighed and recorded. The grain-size curve was determined according to standard D422-63 [17]. The effective size ( $D_{10}$ ), median grain diameter ( $D_{50}$ ) uniformity coefficient ( $C_u$ ) and the coefficient of gradation ( $C_c$ ) were then estimated from the gradational curve. A PVC pipe with dimensions, 0.3 cm thick, 40 cm long and diameter of about 2.7 cm, sealed at the bottom and perforated in the form of a screen with tiny holes (1.0 cm apart) at the sides was driven into the coastal sand formation to a depth of 10 cm from the surface and at a distance of 39 cm away from the wall of the experimental tank to serve as an injection point and simulating leaking underground storage tank or pipeline. The porous material was then saturated with 20 liters of freshwater and was allowed for 2 days to

attain equilibrium. The physical properties of freshwater (TDS = 309  $\mu$ S/cm, EC=231.75 mg/l, Temperature = 28.9°C and pH= 6.1) was determined prior to the usage using the PCTestr-35 multi-Parameter. To serve as control, pre-impact resistivity profiles with dipole-dipole array were acquired for electrode spacing of 2 cm (orthogonal traverses) and 4 cm (main traverses) using a digital Campus Ohmega Resistivity meter by introducing a direct current of 5 mA. The measurements were restricted to 9 cm and 17 cm away from the wall of the wooden tank along the main and orthogonal traverses respectively, to avoid wall effect. The lengths of the orthogonal and parallel traverses are 48 cm and 112 cm respectively (Fig. 1). Controlled injection of 10 liters of crude oil was undertaken. The injection was done over a regular interval for a period of 3 days and at a rate of 0.138 l/hr before measurements was made along the seven traverses. The same electrode array and spacing parameter was utilized for the simulation of both background and crude oil impacted environment. The results obtained were subsequently inverted and plotted as a 2-D resistivity image.

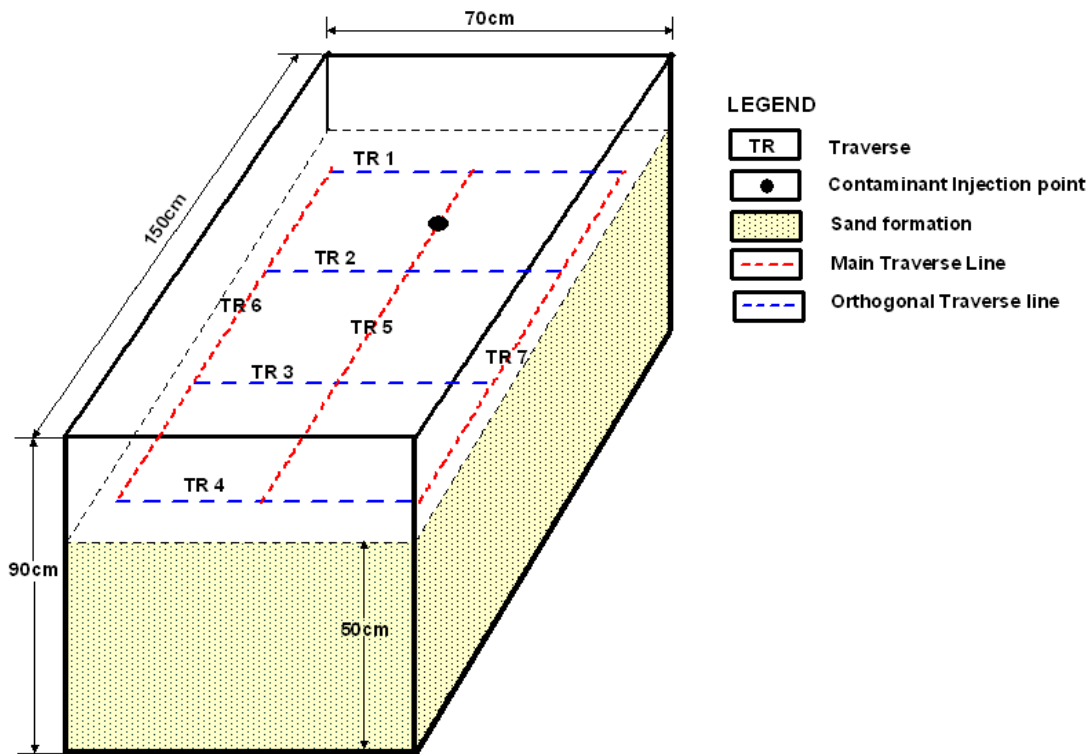


Fig. 2a. Schematic of the laboratory model tank showing measurement traverses

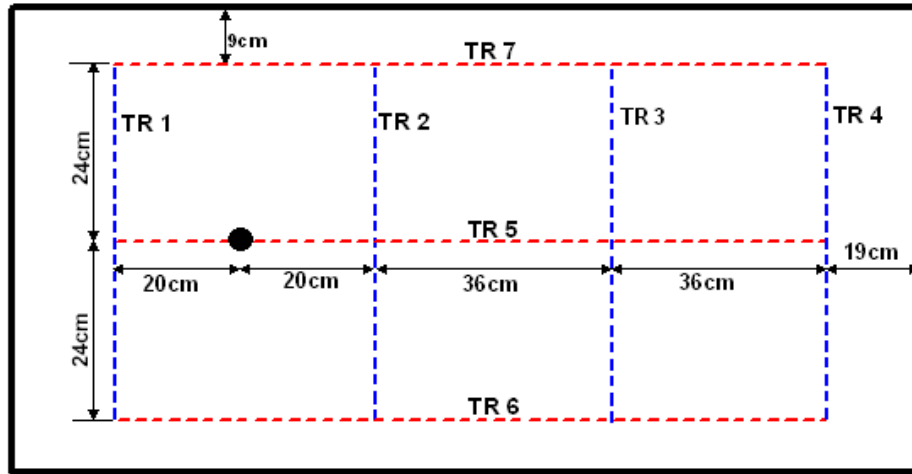


Fig. 2b. Top view of traverse layout for the pre- and post injected sand formation

### 3. RESULTS AND INTERPRETATION

#### 3.1 Textural Characterization

The grain size analysis was performed to determine the percentage of different grain sizes contained within the soil and it was also required to classify the soil. The textural parameters were essential to establish quantitative relationships between physical properties, in this case electrical resistivity and hydraulic properties. The particle size controls the surface electrical conductivity, which increases if the particle size decreases and is predominant for clay [18]. The plot of the grain-size distribution curve of a representative sample of the coastal sand was presented in Fig. 3. The distribution showed characteristics of a well sorted (poorly-graded in engineering terms) soil with a range of particle sizes from fine to medium sand (0.063-1.00 mm). The sample consisted of 98.8% sand and 1.2% fines and has values of 0.24 mm  $D_{10}$ , 0.40 mm  $D_{30}$ , 0.58 mm  $D_{50}$ , 0.68 mm  $D_{60}$ , 2.83 uniformity coefficient,  $C_u$  and 0.98 coefficient of gradation,  $C_c$ .

#### 3.2 Hydraulic Characterization

Derivations of the hydraulic characteristics of a formation were important properties that provided an insight into the behaviour of contaminants in the subsurface. Understanding the principles of contaminant movement through various media in the subsurface plays a significant role in understanding the contaminant migration patterns [19]. The hydraulic properties

considered in this study were coefficient of permeability and transmissivity.

The hydraulic conductivity of the representative sample estimated from [20]. Empirical relation given as

$$K_s = 1.505[(I_0 + 0.025(d_{50} - d_{10}))^2] \quad (5)$$

where,  $K_s$  is expressed in cm/sec

$I_0$  = x-intercept of the straight line formed by joining  $d_{10}$  and the median grain-size  $d_{50}$  of the grain-size distribution curve (mm). The hydraulic conductivity estimated from this relation empirical relation yields a value of  $6.07 \times 10^{-2}$  cm/sec .

[21] established a non-linear relationship between hydraulic conductivity (K) and apparent resistivity ( $\rho$ ) given as

$$K = 0.0538e^{0.007 \rho} \quad (6)$$

where,  $\rho$  is the apparent resistivity of the coastal sand formation. The calculated hydraulic conductivity of the pre-impacted sand ranges between  $1.07 \times 10^{-4}$  and  $7.13 \times 10^{-4}$  m/sec. These hydraulic conductivity values were characteristics of the acquired pre-injection resistivity of the sand which ranged between 95 - 359 $\Omega$ m. Generally, all the values fell within the range of  $10^{-3}$  and  $10^{-1}$  cm/sec for fine to medium sand and the difference indicated characteristic heterogeneity in soil chemistry and porosity.

$$\text{The transmissivity, } T = Kb \quad (7)$$

where K is the hydraulic conductivity value obtained from Singh estimation and b is the thickness of the sand in the model tank yields values ranges between  $5.35 \times 10^{-5}$  and  $3.57 \times 10^{-4}$  m<sup>2</sup>/sec which indicated that the porous medium is prolific aquifer material that is vulnerable to pollution.

### 3.3 Baseline/Pre-injection Electrical Resistivity Image Obtained along the Lines

The pre-injection apparent resistivity pseudosection obtained for traverse 1, 2, 3 and 4 were presented in Figs. 4, 5, 6 and 7. The measured pseudosection for traverse 1 (Fig. 4a), shows a relatively low apparent resistivity ranging from 99 Ωm to 183 Ωm across the section. This resistivity low is constraint at relatively shallow depth. This is an indication that the top layer is more saturated compared to the materials at depth. The 2-D model revealed that this relatively low resistivity zone is restricted at a depth of 0 - 0.01 m and the zone of relatively high resistivity (260 Ωm-350 Ωm) is at depth of 0.02 m beyond (Fig. 4b) The high resistive zone indicates the presence of more sandy materials.

The apparent resistivity pseudosection for traverse 2 shows similar signatures with that of traverse 1 having a relatively low resistivity (148

Ωm-178 Ωm) near the surface compared to the materials at depth (Fig. 5a). This indicates that the near surface materials have low hydraulic conductivity (more clay) and thus impedes the flow of the water to other parts along this line. The corresponding 2-D model shows that this low resistivity zone is limited to a depth of 0-0.02 m across the section (Fig. 5b). In addition, the low resistivity seen at between station position 7 and 11 and at depth of 0.07 m indicates the concentration of clayey sand at this zone. The layer of high resistivity (>318 Ωm) seen between 0.04 m-0.06 m depth across the section suggest the occurrence of more sandy materials. A comparison of the recovered resistivity images of traverses 1 and 2 shows the non-uniformity of the sediments in the tank.

Comparatively to traverse 1 and 2 (Figs. 4 and 5), line 3 shows a more pronounced low resistivity signature which indicate relatively more saturated top soil across this section (Fig. 6a and b). It is seen from the 2-D inverted model that the low resistivity zone occurs from the left side to station position 15 and at depth of 0.00 m-0.03 m and at station position 15- 22 at a depth of 0.03 m beyond across the section (Fig. 6b). This suggests that the water has migrated through preferential path ways (sandy materials) to this region. The resistivity high (>319 Ωm) seen at between station position 5 - 8 and 12 - 16 and at

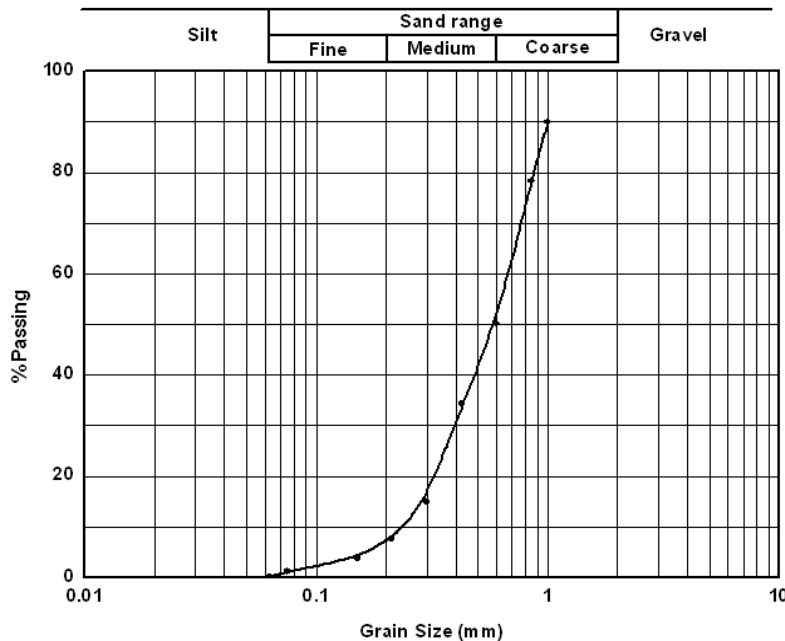
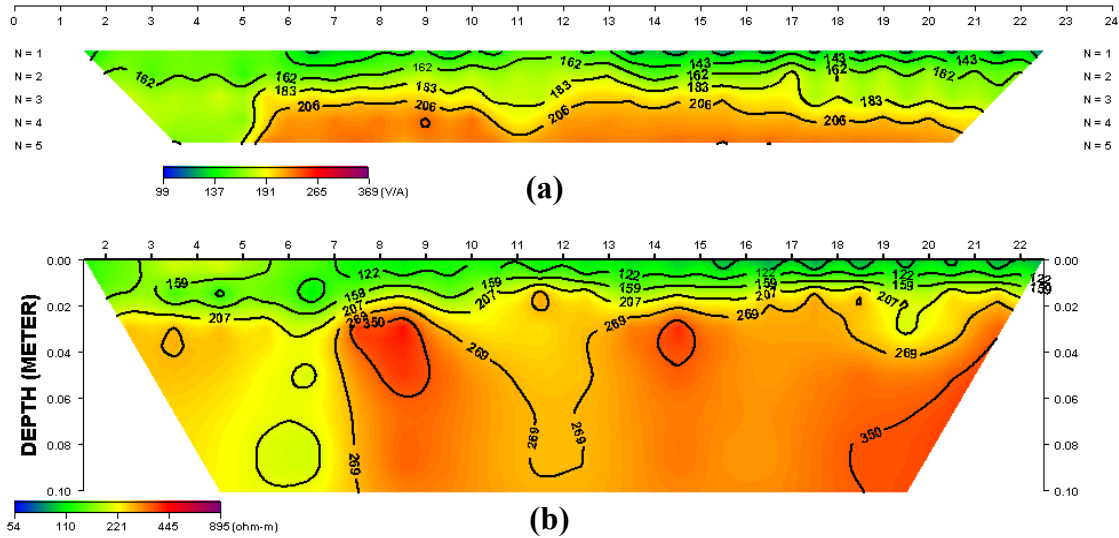


Fig. 3. Grain-size distribution curve of the representative coastal sand sample



**Fig. 4. The recovered 2-D resistivity model from the inversion of the pre-injection resistivity data of TR 1. Upper panel shows the acquired laboratory data and the lower panel, the equivalent 2-D model. The RMS error converges to 6.4% from 18.54% after the tenth iteration**

depth of about 0.03 m beyond implies that this area is partially saturated or possibly has more resistive materials (sand) compared to other zones.

The image obtained for traverse 4 shows a relatively low resistivity (less than 168  $\Omega$ m) zone occurring near the surface compared to the once at depth across the section (Fig. 7a). This indicates high degree of saturation of the topmost materials compared to those at depth (resistivity value greater than 230  $\Omega$ m). The inverted 2-D structure (Fig. 7b), revealed more heterogeneity of the sand formation along this line compared to traverse 1, 2 and 3 (Figs. 4, 5 and 6). Evidence from the geo-electrical model, revealed that the low resistivity (less than 211  $\Omega$ m) zone is limited to a depth of 0.06 m at the left side, 0.02 m at the center and 0.04 m towards the right side of the section. This indicates that the water has migrated more towards the left side possibly because of the presence of more sandy materials in this zone. The concentration of high resistivity (>418  $\Omega$ m) materials seen at between station position 5 - 11 and at depth of about 0.05m beyond can be interpreted as the concentration of more resistive (sand) material and subsequently leading to the easy movement of the water towards this region. However, the resistivity low which occurs at between station positions 12 - 15 at the topmost part of the section indicates the presence of clayey topsoil.

The apparent resistivity pseudosection and 2-D image obtained along the main traverses (5, 6 and 7) is presented in Figs. 8, 9 and 10. The pseudosection obtained for traverse 5 shows a low resistivity (<146  $\Omega$ m) at the left side compared to the right side (>256  $\Omega$ m) of the section (Fig. 8a). This suggests higher degree of saturation or possibly the presence of high conductive materials (clay) in this zone compared to the right side. The 2-D model shows a resistivity low (as low as <101  $\Omega$ m) at between station position 5 - 8 and at depth of 0.10 m beyond (Fig. 8b). This indicates the presence of more clay materials in this zone. The high resistivity (>295  $\Omega$ m) seen at between station position 9 - 13 and at depth of 0.12 m beyond as well as some pockets of high resistivity at between station position 15 - 23 and at depth of about 0.02 m to 0.08 m suggest the occurrence of more sandy materials in this zone. In comparison, to traverse 5, the right side of traverse 6 seems to be less saturated possibly due to presence of low hydraulic conductivity (high clay content) material in this zone (Fig. 9a). The associated subsurface image shows that these materials are more pronounced at between station position 2 - 5, near the surface and at depth of 0.08 m beyond, between station position 7 - 15 and at depth of 0.03 m to 0.07 m, and between station 18 - 21 and at depth of 0.08 m beyond respectively (Fig. 9b). The resistivity high (>329  $\Omega$ m) seen at between station position 7 - 13 and at depth of about 0.10 m beyond

indicates occurrence of more resistive material (lower clay content). The image obtained along traverse 7 shows a low resistivity zone occurring between stations position 11 - 21 and this may indicate high degree of saturation along the section (Fig. 10a). The subsurface image shows pockets of high resistivity ( $>298 \Omega\text{m}$ ) closures between station position 6 and 10 and at depth of 0.04 m to 0.08 m (Fig. 10b). The high resistivity zone also, seen at between station position 14 - 17 and at depth of about 0.07 m beyond and towards the right side at depth of 0-

0.16 m suggest the presence of more sandy materials in these zones.

### 3.4 Post-Crude Oil Injection Electrical Resistivity Images along the Profiles

The apparent resistivity pseudosection obtained for traverse 1, 2, 3 and 4 are presented in Figs. 11, 12, 13 and 14. The pseudosection obtained along line 1 done 4,320 mins after crude oil injection shows no evidence of its impact along this section (Fig. 11a). This implies that the

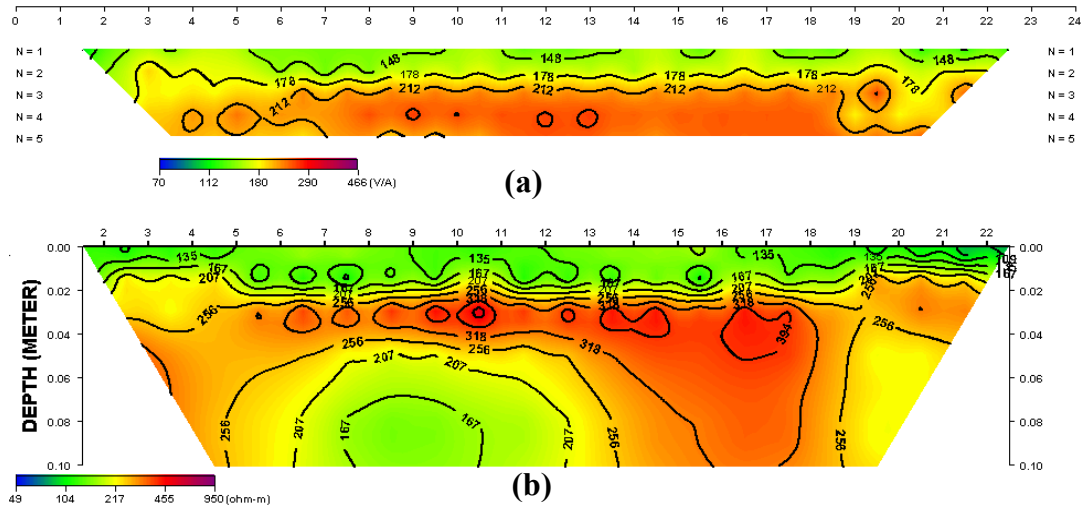


**Fig. 5.** The 2-D resistivity structure obtained from inversion of the pre-injection resistivity data measured on TR 2. Upper panel shows the acquired laboratory data and the lower panel, the equivalent 2-D model. The RMS error converges to 7.8% from 12.03% after the tenth iteration

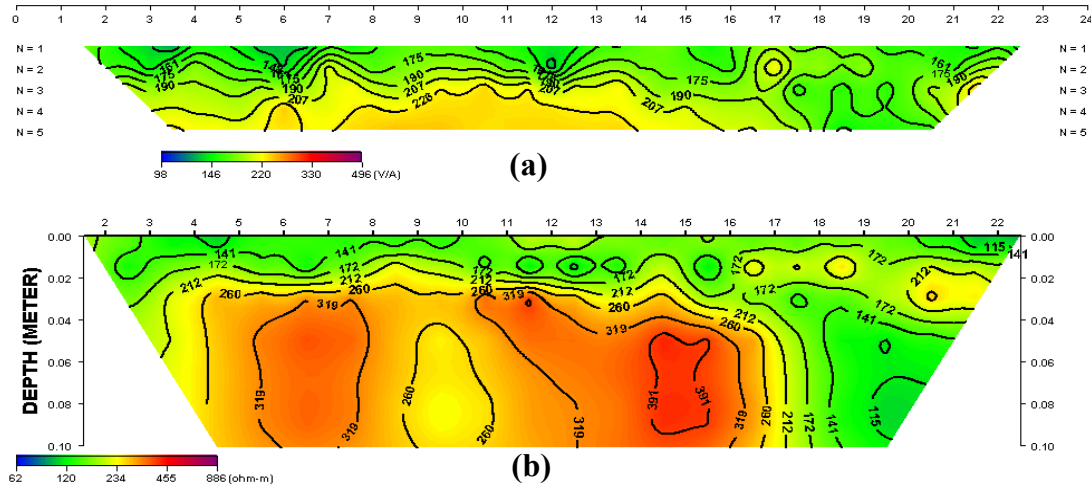


**Fig. 6.** The 2-D resistivity structure recovered from inversion of the pre-injection resistivity data obtained on TR 3. Upper panel shows the acquired laboratory data and the lower panel 2-D model. The RMS error converges to 6.4% from 19.01% after the tenth iteration

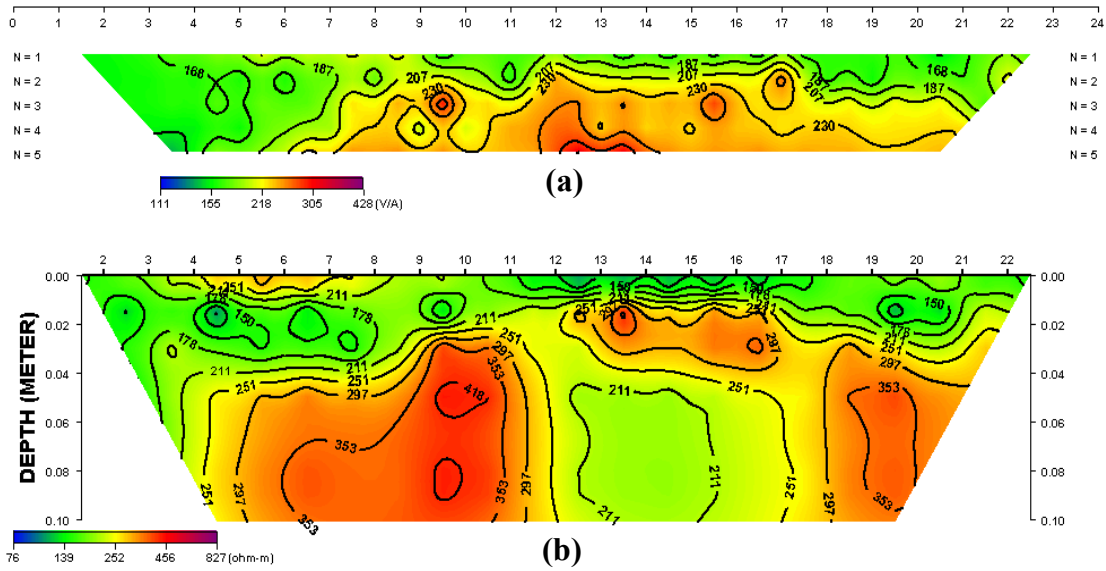


**Fig. 7. The 2-D resistivity model recovered from inversion of the pre-injection resistivity data obtained on TR 4. Upper panel shows the acquired synthetic laboratory data and the lower panel corresponding 2-D model. The RMS error converges to 5.2% from 10.37% after the tenth iterations**

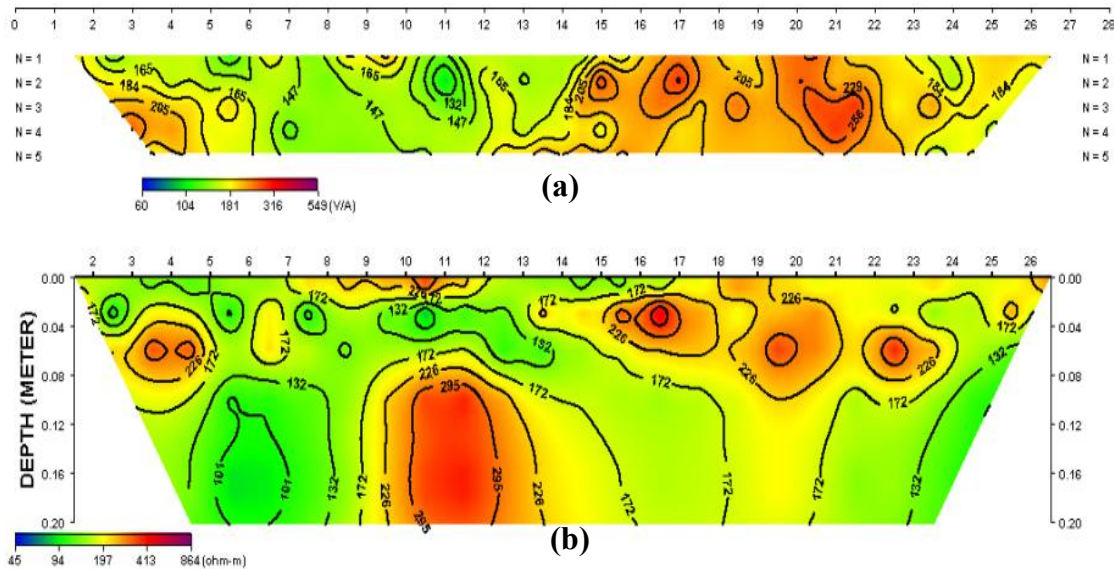


**Fig. 8. The 2-D resistivity model recovered from inversion of the pre-injection resistivity data obtained on TR 5. Upper panel shows the acquired synthetic laboratory data and the lower panel, 2-D model. The RMS error converges to 6.2% from 14.05% after the tenth iteration**

hydrocarbon has not moved towards this zone (20 cm away from injection point). The 2-D image revealed a relatively low resistivity (less than 235  $\Omega\text{m}$ ) at between station positions 9-13 near the surface (Fig. 11b). This possibly suggest that the freshwater used to saturate the material is yet to infiltrate that far due to low hydraulic conductivity

materials (more clay content) around this area. However, after about 4,388 min of injection, the measured pseudosection for traverse 2 revealed the impact of the crude oil along this line (Fig. 12a) between station positions 9 - 14 with resistivity reading as high as 950  $\Omega\text{m}$  compared to the materials at depth ( $< 558 \Omega\text{m}$ ). The

inverted 2-D image shows that the plume (>1096  $\Omega\text{m}$ ) is restricted within shallow (0.04 m) depth and at between station position 8-14 which implies that the crude oil is yet to migrate to greater depth possible due to the presence of more clay materials beneath the vicinity of its

accumulation (Fig. 12b). About 4,450 min after injection the apparent resistivity pseudosection obtained along traverse 3 shows the evidence of the crude oil impacted zone between station number 8 - 12 and at relatively shallow depth (Fig. 13a). The 2-D image revealed a clear

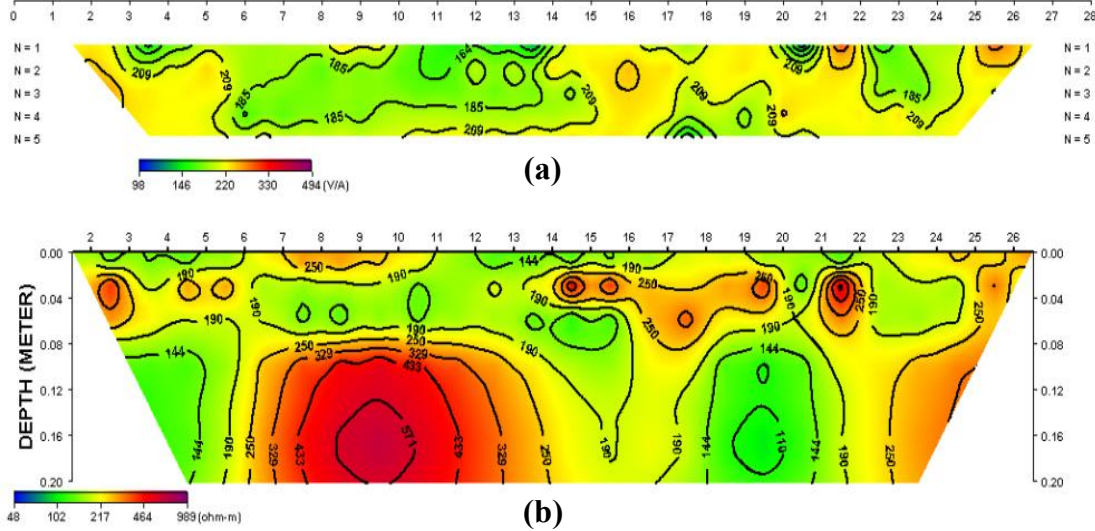


**Fig. 9.** The 2-D resistivity model recovered from inversion of the pre-injection resistivity data obtained on TR 6. Upper panel shows the acquired laboratory data and the lower panel, 2-D model. The RMS error converges to 7.9% from 19.21% after the tenth iteration

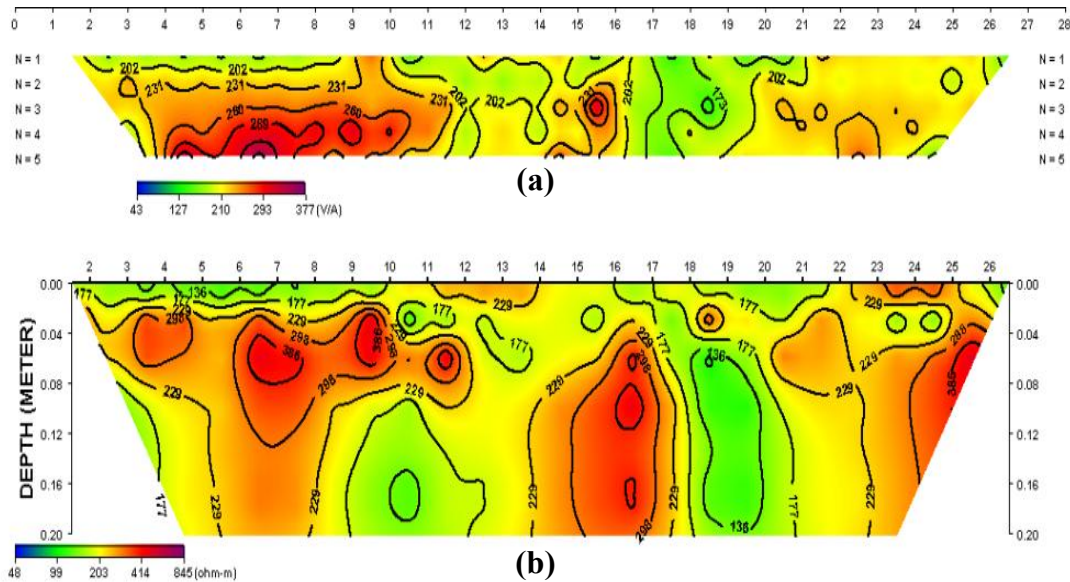


**Fig. 10.** The 2-D resistivity model recovered from inversion of the pre-injection resistivity data obtained on TR 7. Upper panel shows the acquired laboratory data and the lower panel, 2-D model. The RMS error converges to 7.9% from 19.21% after the tenth iteration

evidence of the lateral spread of the crude oil plume (Fig. 13b) with resistivity value as high as 1547  $\Omega\text{m}$  occur between station positions 8-13 at depth of 0.01 m beyond and some pockets (>965  $\Omega\text{m}$ ) of the crude occurring at the towards the right and left side of the section. However, from

the apparent resistivity pseudosection (Fig. 14a) and the corresponding 2-D model (Fig. 14b) obtained along line 4, 4,516 mins after injection, it is clear that, the crude oil did not migrate towards this region possibly because its farther (92 cm away) from the injection point.

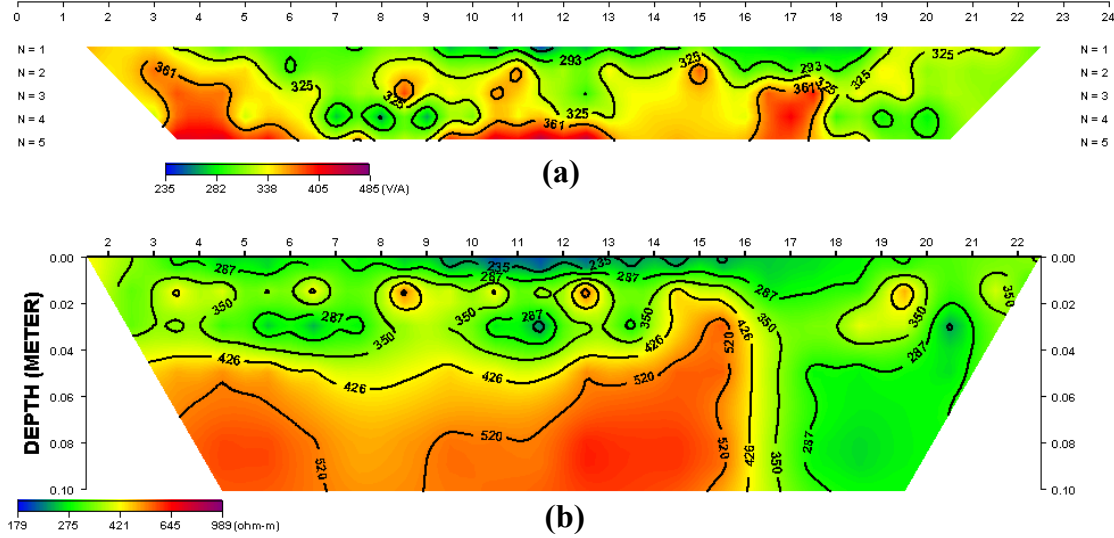


**Fig. 11. Post-injection 2D resistivity image beneath traverse TR 1 (4,320 min after crude oil injection). The upper and lower panels show the laboratory data and the corresponding 2D resistivity model obtained through inversion. The RMS error of the 2D model converges to 6.7% from 11.02% after the tenth iteration**

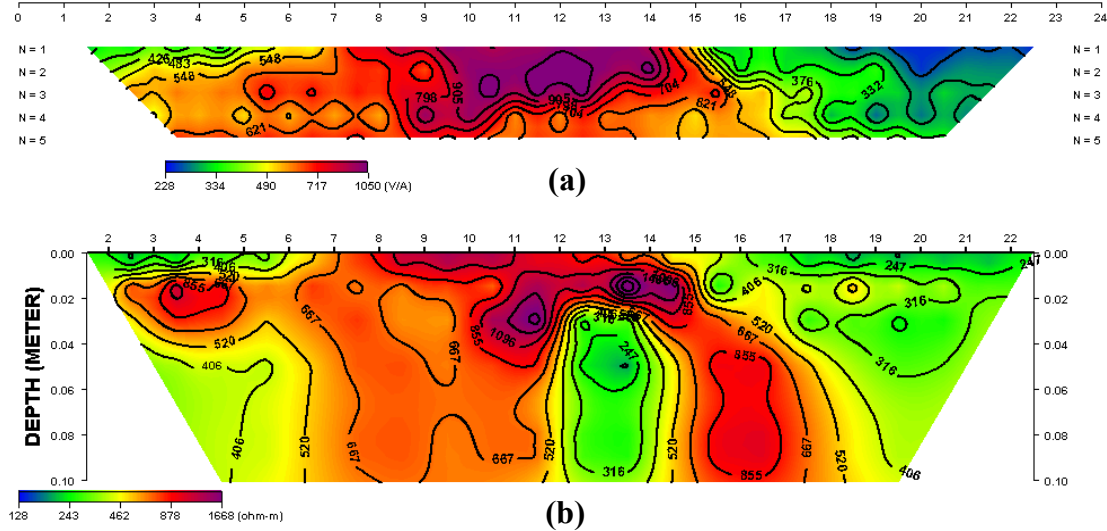


**Fig. 12. Post-injection 2D resistivity image beneath traverse TR 2 (4,388 min after crude oil injection). The upper and lower panels show the laboratory data and the corresponding 2D resistivity data obtained through inversion. The RMS error of the 2D model converges to 5.2% from 14.12% after the tenth iteration**

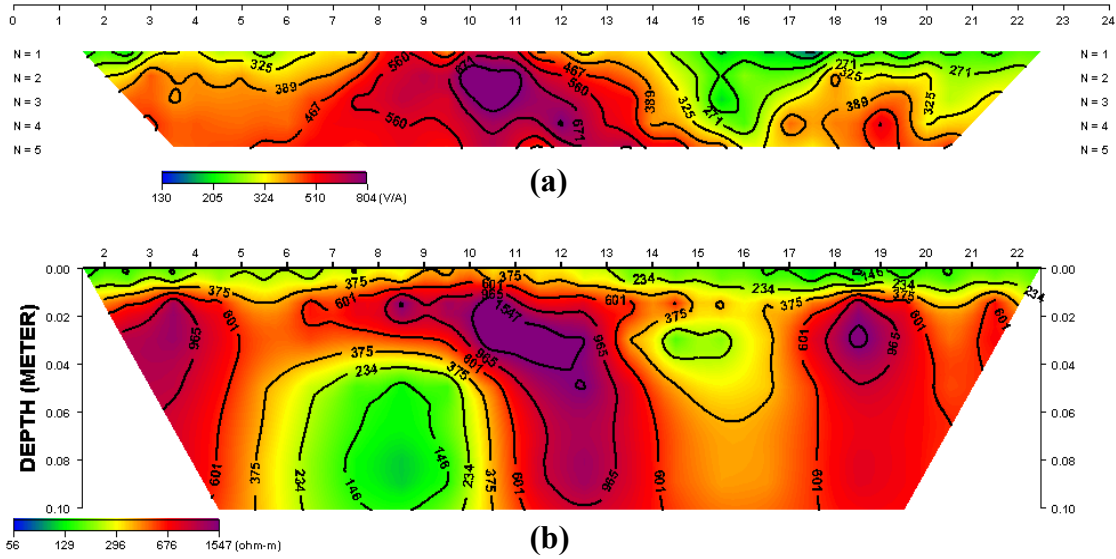


**Fig. 13.** Post-injection 2D resistivity image beneath traverse TR 3 (4,450 min after injection). The upper and lower panels show the laboratory data and the corresponding 2D resistivity model obtained through inversion. The RMS error of the 2D model converges to 8.3% from 12.12% after the tenth iteration

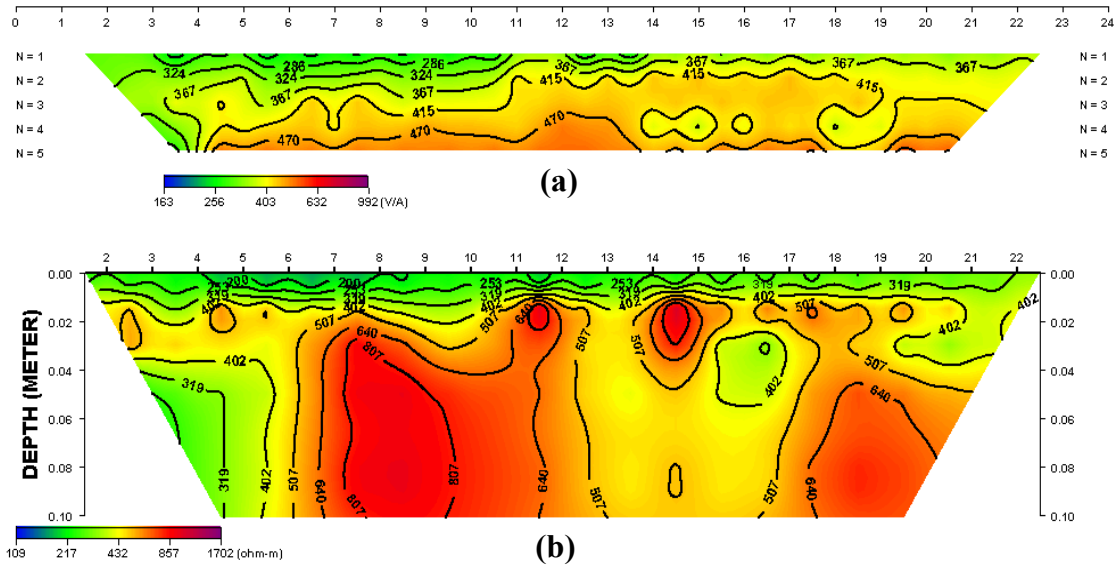


**Fig. 14.** Post-injection 2D resistivity image beneath traverse TR 4 (4,516 min after injection). The upper and lower panels show the laboratory data and the corresponding 2D resistivity model obtained through inversion. The RMS error of the 2D model converges to 7.5% from 11.33% after the tenth iteration

The apparent resistivity pseudosection and its associated subsurface image obtained for the main lines are presented in Figs. 15, 16 and 17. The pseudosection for traverse 5 done 4,578 mins after injection revealed a high resistivity anomaly (>973  $\Omega$ m) between station number 3 - 12 which signifies the influence of the crude oil

within this zone as compared to the right side (low resistivity) of the section (Fig. 15a). Apart from the fact that the features in the observed pseudosection is significantly preserved in the inverted 2-D model, distinct resistivity high (as high as 2064  $\Omega$ m) at between station number 4 and 8 and at depth of 0.00 to 0.03 m as well as

at between station position 6 - 12 and at a depth of 0.05 m beyond was delineated along this line (Fig. 15b). The increase in resistivity values from the near surface materials to the materials at depth ( $>3139 \Omega\text{m}$ ) is a clear evidence that the plume is migrating towards the base of the sand tank below the release point. This observed anomaly in the partially saturated system probably may have resulted from the replacement of the air-water interface in the pores of the material with a hydrocarbon-water interface.

The apparent resistivity pseudosection obtained for traverse 6 (4,643 mins after injection) revealed a high resistivity ( $>1261 \Omega\text{m}$ ) anomaly at between station position 9 - 15 at a significantly shallow depth (Fig. 15a). The high resistivity values associated with this zone is 14 - 16% increase over the baseline resistivity values. The resistivity low (as low as  $544 \Omega\text{m}$ ) seen towards the right side of the section implies no impact of the injected crude oil on this zone. The 2-D model shows a relatively low resistivity values ( $<502 \Omega\text{m}$ ) from 0.00 - 0.05 m depth

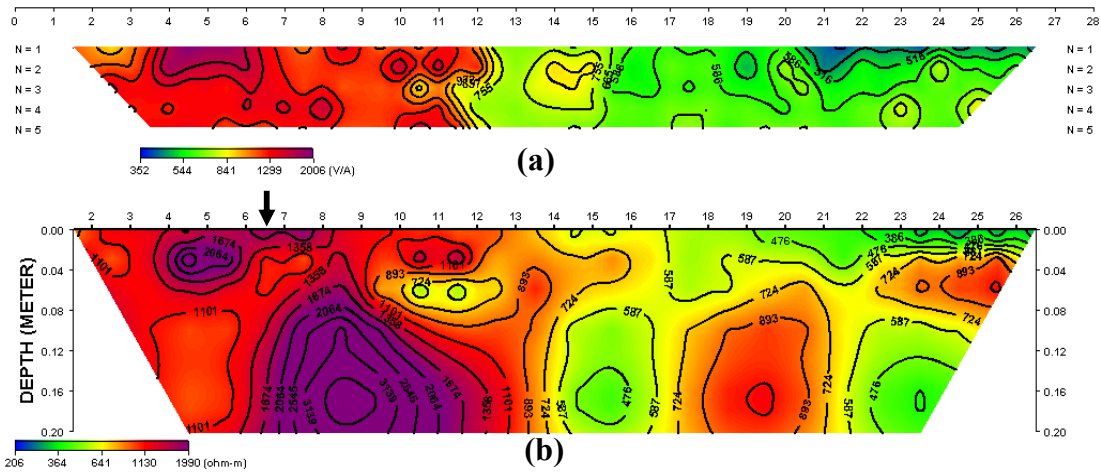


**Fig. 15.** The 2-D image of the crude oil lens obtained for TR 5 (4,578 mins after injection). The upper panel is the laboratory data and the lower panel shows the 2D resistivity structure beneath the traverse. The RMS error of the model converges to 7.8% from 14.03% after the tenth iteration. Arrow indicates injection point

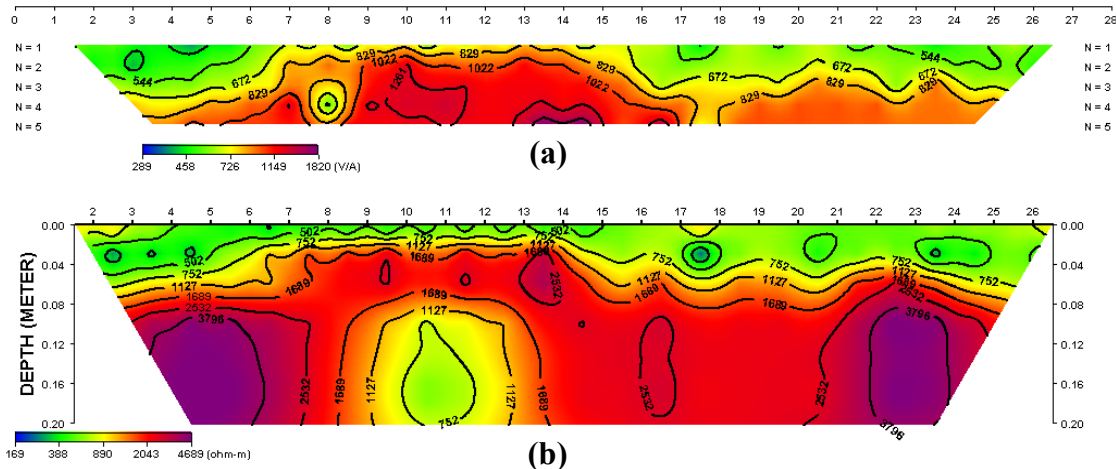


**Fig. 16.** The 2-D image of the crude oil lens obtained for TR 6 (4,643 min after injection). The upper panel is the laboratory data and the lower panel shows the 2D resistivity structure beneath the traverse. The RMS error of the model converges to 9.8% from 15.7% after the tenth iteration

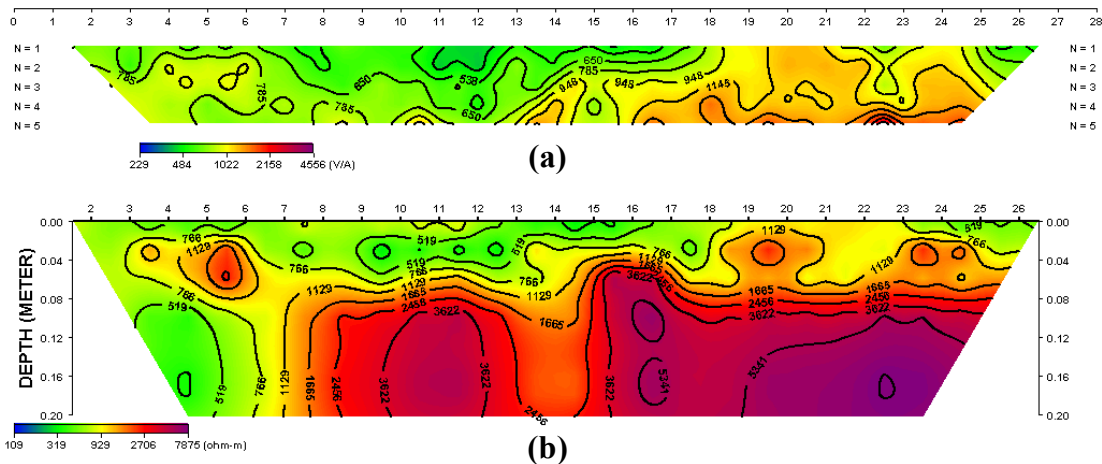


**Fig. 17. The 2-D inversion synthetic dipole-dipole resistivity data of the crude oil lens obtained for TR 7 (4,707 min after injection). The upper panel is the laboratory data and the lower panel shows the 2D resistivity structure beneath the traverse. The RMS error of the model converges to 7.5% from 15.47% after the tenth iteration**

across the section (Fig. 15b). However, a general increase in resistivity values especially at the lower part, between station positions 2 - 7 and 21 to 24.5 at depth of 0.10 m beyond indicates that the hydrocarbon plume has spread laterally to this zone. The presence of the crude oil plume appears to be much more pronounced compared to traverse 5 because more time has elapsed before the data was acquired along this line. 4,707 mins after injection of the crude oil, no evidence of its impact was seen in measured apparent resistivity pseudosection of traverse 7 (Fig. 17) which is an indication that the hydrocarbon has pooled at the bottom of the experimental sand tank. The 2-D image further confirmed this observation as the plume is seen to have accumulated at between station positions 9 - 13 and 15 - 26 at a depth > 0.10 m.

#### 4. SUMMARY AND CONCLUSION

A laboratory simulation of hydrocarbon spill delineation in coastal sands by Electrical resistivity was successfully carried out. Textual and hydraulic characterization showed that the porous medium was a well sorted fine to medium grain sand with calculated hydraulic conductivity (K) values ranging between  $1.07 \times 10^{-4}$  and  $7.13 \times 10^{-4}$  m/sec and transmissivity (T), ranging between  $5.35 \times 10^{-5}$  and  $3.57 \times 10^{-4}$  m<sup>2</sup>/sec which implies that the coastal sand is vulnerable to pollution. Pre-injection inverted data obtained for all the traverses, revealed that the porous medium exhibits heterogeneity which was more pronounced on traverse 5, 6 and 7 compared to

traverse 1, 2, 3, and 4. The images obtained along the orthogonal lines in the saline water and crude oil simulation showed that the high resistive anomaly reflected the presence of the crude oil plume within the coastal sand medium. However, the values of this anomaly were slightly reduced compared to what was expected for a hydrocarbon anomaly due to the influenced of the saline water. Images obtained showed that the resistive anomaly that developed suggested the displacement of capillary conductive water by increased hydrostatic pressure, replacing the air with crude oil in the water-wet system. This mechanism seemed to be more pronounced towards the right side of traverse 7 compared to traverse 6. Also a comparison between the apparent resistivity pseudosection data calculated from the 2-D model and the respective observed data indicates that most of the features in the laboratory data are accurately modeled. Although, these models are not necessarily unique, as other models could probably produce acceptable fits to the observed data. The response of the crude oil was imaged as high apparent resistivity anomaly in the partially saturated soil. It is evident from the images obtained that the impact of the crude oil was restricted to traverse 2 and 3 along the orthogonal lines which implies that the migration of the plume was towards the right side of the model tank. The resistivity signatures obtained along the main lines, revealed that the migration of the hydrocarbon plume was more prominent along the sides (traverse 6 and 7) of the model tank possibly because these regions have high

hydraulic conductivity materials (sandy materials) and/or is less saturated within the model tank. Also, in comparison to the orthogonal lines (traverse 1, 2, 3 and 4) the impact of the crude oil was clearly delineated along all the main traverses possibly because more time has elapsed before the data was acquired. However, the crude oil plume was restricted below the released point in line 5 but was seen to have spread significantly to greater distance in line 6 and 7. This study demonstrates the application of geophysics in hydrocarbon spill delineation in coastal sands environment as prevalent in the Niger Delta region of Nigeria, results show the effectiveness of this method in the design of efficient hydrocarbon spill cleanup programmes.

### COMPETING INTERESTS

Authors have declared that no competing interests exist.

### REFERENCES

1. Ozumba CI, Ozumba MB, Obobaifo CE. Striking a balance between oil exploration and protecting the environment: The SPDC experience. *NAPE Bulletin*. 1999;14(2): 130-135.
2. Ramirez A, Daily W, LaBrecque D, Owen E, Chesnut D. Monitoring an underground steam injection process using electrical resistance tomography. *Water Resour Res*. 1993;29:73-87.
3. Frohlich RK, Urish DW, Fuller J, Reilly MO. Use of geoelectrical method in groundwater pollution surveys in a coastal environment. *Journal of Applied Geophysics*. 1994;32:132-154.
4. Barker RD. Electrical imaging and its application in engineering investigations. In: *Modern Geophysics in Engineering Geology* (ed. D. Mcann). Special Publication of the Geological Society; 1996.
5. Okereke CS, Esu EO, Edet AE. Determination of potential groundwater sites using geological and geophysical techniques in the Cross River State, southeastern Nigeria. *Journal of African Earth Sciences*. 1998;27(1):149-163.
6. Sauck WA, Atekwana EA, Nash MS. A conceptual model for the geoelectrical response of LNAPL plumes in granular sediments. *Proceedings of SAGEEP*. 1998;805-817.
7. Atekwana EA, Sauck WA, Werkema DD. Investigations of geoelectrical signatures at a hydrocarbon contaminated site. *Journal of Applied Geophysics*. 2000;44:167-180.
8. Choudhury K, Saha DK, Chakraborty P. Geophysical study of saline water intrusion in a coastal alluvial terrain. *Journal of Applied Geophysics*. 2001;46:189-200.
9. Garcia MG, Hidalgo M. del V, Belsa MA. Geochemistry of groundwater in the alluvial plain of Tucuman province, Argentina. *Hydrogeology*. 2001;9:597-610.
10. Maza`c O, Kelly WE, Landa I. Surface geoelectrics for groundwater pollution-survey design. *J Hydrol*. 1989;111:163-176.
11. Fukue M, Taya N, Matsumoto M, Sakai G. Development and application of cone for measuring the resistivity of soil. *Journal of Geotechnical Engineering, Japanese Society of Civil Engineers*. 1998;596(3-43): 283-293. (Text in Japanese)
12. Fukue M, Minato T, Matsumoto M, Horibe H, Taya N. Use of resistivity cone for detecting contaminated soil layers. *Eng. Geol*. 2001;60:361-369.
13. Godio A, Naldi M. Two-dimensional electrical imaging for detection of hydrocarbon contaminants. *Near Surf Geophys*. 2003;1:131-137.
14. Atekwana EA, Sauck WA, Werkema DD Jr. Characterization of a complex refinery groundwater contamination plume using multiple geoelectrical methods. In: *Proceedings the Symposium on the Application of Geophysics to Engineering and Environmental Problems, EEGS, Chicag*. 1998;427-436.
15. Maza`c O, Benes L, Landa I, Maskova A. Determination of the extent of oil contamination by geoelectrical methods. *Geotech Environ Geophys Environ Groundwater*. 1990;2:107-112.
16. Yi MJ, Kim JH, Song Y, Cho SJ, Chung SH, Suh JH. Three-dimensional imaging of subsurface structures using resistivity data. *Geophys Prospect*. 2001;49(4):483-497.
17. ASTM. Standard method for particle-size analysis of soils (D422-63). In *1991 Annual Book of ASTM Standards*. 1991c;4(8):87-96.
18. Frohlich RK, Urish DW. The use of geoelectrics and test wells for the assessment of groundwater quality of a coastal industrial site. *Journal of Applied Geophysics*. 2002;50:261-278.

19. Bedient PB, Rifai HS, Newell CJ. Groundwater contamination, transport and remediation. 2nd Edn. Prentice Hall, London. 1999;24–33.
20. Alyamani MS, Sen Z. Determination of hydraulic conductivity from complete grain-size distribution curves. Groundwater. 1993;31(4):551-555.
21. Singh KP. Non-linear estimation of aquifer parameters from surficial resistivity measurements. Hydrol Earth Syst Sci Discuss. 2005;2:917–938.

---

© 2018 Sualla et al.; This is an Open Access article distributed under the terms of the Creative Commons Attribution License (<http://creativecommons.org/licenses/by/4.0>), which permits unrestricted use, distribution, and reproduction in any medium, provided the original work is properly cited.

*Peer-review history:*  
*The peer review history for this paper can be accessed here:*  
<http://www.sciencedomain.org/review-history/22835>